Predissociation dynamics of N2O+ at the A2Σ+ state: Three pathways to form NO+(1Σ+) revealed from ion velocity imaging

Hua Wang, Xiaoguo Zhou, Shilin Liu, Bo Jiang, Dongxu Dai et al.

Citation: J. Chem. Phys. **132**, 244309 (2010); doi: 10.1063/1.3457945
View online: http://dx.doi.org/10.1063/1.3457945
View Table of Contents: http://jcp.aip.org/resource/1/JCPSA6/v132/i24
Published by the American Institute of Physics.

Predissociation dynamics of N_2O^+ at the $A\ ^2\Sigma^+$ state: Three pathways to form $NO^+(^1\Sigma^+)$ revealed from ion velocity imaging

Hua Wang (汪华),[1] Xiaoguo Zhou (周晓国),[1] Shilin Liu (刘世林),[1,a)] Bo Jiang (姜波),[2] Dongxu Dai (戴东旭),[2] and Xueming Yang (杨学明)[2]
[1]*Department of Chemical Physics, Hefei National Laboratory for Physical Sciences at the Microscale, University of Science and Technology of China, Hefei, Anhui 230026, China*
[2]*State Key Laboratory of Molecular Reaction Dynamics, Dalian Institute of Chemical Physics, Chinese Academy of Sciences, Dalian, Liaoning 116023, China*

(Received 15 April 2010; accepted 8 June 2010; published online 28 June 2010)

The predissociation dynamics of nitrous oxide ion (N_2O^+) at its first excited state $A\ ^2\Sigma^+$ has been investigated with ion velocity imaging by probing the NO^+ fragments. The parent ion N_2O^+, prepared at the ground state $X\ ^2\Pi(000)$ through (3+1) resonance-enhanced multiphoton ionization (REMPI) of jet-cooled N_2O molecules at 360.55 nm, was excited to different vibrational levels of the $A\ ^2\Sigma^+$ state in a wavelength range of 280–320 nm, and then predissociated to form NO^+ and N fragments. The internal energy distribution of the NO^+ fragment was determined from its ion velocity images. With the help of potential energy surfaces (PESs) of N_2O^+, three dissociation pathways have been proposed to interpret the three kinds of NO^+ fragments with different internal state distributions: (1) the $A\ ^2\Sigma^+$ state couples to a dissociative $1\ ^4\Sigma^-$ state via a bound $1\ ^4\Pi$ state to form the $NO^+ + N(^4S)$ channel, where NO^+ fragment is rotationally hot; (2) the $A\ ^2\Sigma^+$ state couples to dissociative states $^2\Sigma^-/^2\Delta$ via the $1\ ^4\Pi$ state to form the $NO^+ + N(^2D)$ channel, where NO^+ fragment is also rotationally hot; (3) the $A\ ^2\Sigma^+$ state couples to the high energy region of the ground state $X\ ^2\Pi$ and then dissociates to form the $NO^+ + N(^2D)$ channel, where NO^+ is rotationally cold. © *2010 American Institute of Physics*. [doi:10.1063/1.3457945]

I. INTRODUCTION

One of the most important reactions in the upper atmosphere of the earth is an exothermic ion-molecule reaction,[1–6]

$$O^+(^4S) + N_2(X\ ^1\Sigma^+) \rightarrow NO^+(X\ ^1\Sigma^+) + N(^4S) + 1.099\ \text{eV}. \quad (1)$$

For this reaction, N_2O^+ molecular ion was found to be the intermediate product which plays a essential role in the reaction mechanism and the final product state distributions. Extensive theoretical[7–15] and experimental[16–38] studies had been performed on the structure and dynamics of the N_2O^+ ion, mainly for its electronic ground state $X\ ^2\Pi$ and the first electronically excited state $A\ ^2\Sigma^+$. Various experimental methods had been utilized, such as fluorescence emission spectroscopy,[16–21] fast-ion beam laser spectroscopy (FIBLAS),[22–26] photoelectron spectroscopy,[27–29] threshold photoelectron-photoion coincidence (TPEPICO) spectroscopy,[30–33] and photofragment excitation (PHOFEX) spectroscopy.[34–41] For the $X\ ^2\Pi$ state, it had been clear that this is a bound state with linear geometry.[15] Spectroscopic studies had revealed many complex spectroscopic features arising from various interactions, such as the spin-orbit splitting, Renner–Teller interactions, and the Fermi-resonance couplings in the $X\ ^2\Pi$ state.[14–16,19,21,26] The first electronically excited state of N_2O^+, $A\ ^2\Sigma^+$, had also been studied. Fragmentary information about the spectral constants had been obtained from the emission spectroscopic studies on the several lowest vibrational levels of the $A\ ^2\Sigma^+$ state.[16–21] Recently, a systematic study on the PHOFEX spectrum of $N_2O^+(A\ ^2\Sigma^+)$ had been performed by Xu *et al.*[39] over a wide excitation energy range, detailed spectral constants with high precision had been obtained, and the strong Fermi-resonance couplings had been studied between the ν_1, ν_2, and ν_3 vibrational modes.

There are two energetically accessible dissociation channels for $N_2O^+(A\ ^2\Sigma^+)$ from the *ab initio* theoretical calculations,[15] as shown in Fig. 1. One forms $NO^+(X\ ^1\Sigma^+) + N(^4S)$ products with lower dissociation limit [$N(^4S)$ channel], the other forms $NO^+(X\ ^1\Sigma^+) + N(^2D)$ products with higher dissociation limit [$N(^2D)$ channel]. Previous experimental photodissociation studies on $N_2O^+(A\ ^2\Sigma^+)$ were only limited to several lowest vibrational levels.[22–24,31,32] It has been known that these lowest vibrational levels, except for the ground vibrational level (000), undergo predissociation to produce the $N(^4S)$ and $NO^+(X\ ^1\Sigma^+, v)$ fragments. The FIBLAS experiments[23,24] showed that the state distribution of the NO^+ fragments from the $A\ ^2\Sigma^+(100)$ level is vibrationally inverted and centers at v=4. The TPEPICO study at the (100), (001), and (200) levels showed that the NO^+ fragment is mainly populated at v=4 or 5.[31] While for the dissociation of $N_2O^+(A\ ^2\Sigma^+)$ at a higher vibrational level, (300), a quite different state distribution of NO^+ was found,[31] which was interpreted by the possible coexistence of two dissociation channels, forming respectively $NO^+(v=8\ \text{or}\ 9) + N(^4S)$ and

a)Author to whom correspondence should be addressed. Electronic mail: slliu@ustc.edu.cn.

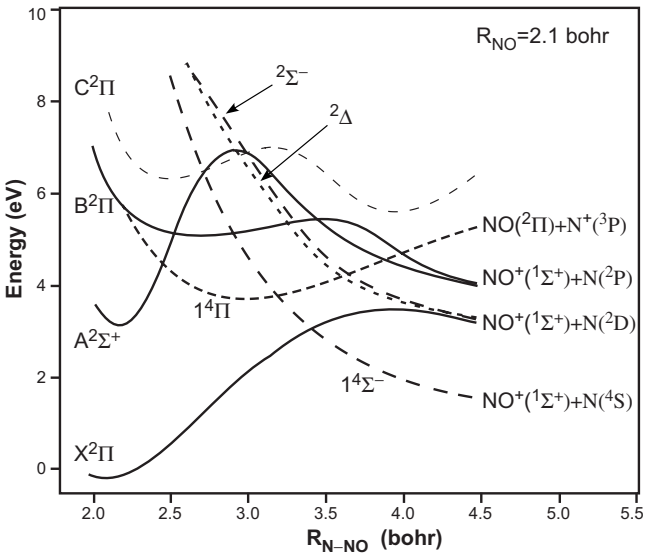

FIG. 1. Potential energy curves of low lying electronic states of N_2O^+ along the N–NO collinear dimension reproduced from Ref. 15.

$NO^+(v=0 \text{ or } 1)+N(^2D)$. Xu *et al.*[40] studied the photodissociation dynamics of $N_2O^+(A\ ^2\Sigma^+)$ in a wide excitation energy range, and found a channel-switching effect by measuring the total released kinetic energies from the time-of-flight mass spectrum. The results showed that with the increase of excitation energy, dissociation pathway of $N_2O^+(A\ ^2\Sigma^+)$ changes abruptly from the $N(^4S)$ channel to the $N(^2D)$ channel at the (300) level. The observation was explained by competition between the two dissociation channels across the special excitation energy region.

The dissociation mechanism of the $N(^4S)$ channel had been theoretically investigated[8–11,15] and is well known as a three-step process, i.e., the $A\ ^2\Sigma^+$ state couples with a bound $1\ ^4\Pi$ state through spin-orbit interaction, and then crosses with a repulsive $1\ ^4\Sigma^-$ state, leading finally to the NO^+ and $N(^4S)$ fragments,

$$N_2O^+(A\ ^2\Sigma^+) \overset{\text{spin-orbit}}{\leftrightarrow} N_2O^+(1\ ^4\Pi) \rightarrow N_2O^+(1\ ^4\Sigma^-) \rightarrow NO^+(X\ ^1\Sigma^+) + N(^4S). \quad (2)$$

The mechanism of the $N(^2D)$ channel, as discussed by Xu *et al.*,[40] was proposed to be a two-step process. The $A\ ^2\Sigma^+$ state interacts with the $X\ ^2\Pi$ state via vibronic coupling, and then dissociates adiabatically from the $X\ ^2\Pi$ state to form NO^+ and $N(^2D)$ fragments,

$$N_2O^+(A\ ^2\Sigma^+) \overset{\text{vibronic coupling}}{\rightarrow} N_2O^+(X\ ^2\Pi) \rightarrow NO^+(X\ ^1\Sigma^+) + N(^2D). \quad (3)$$

Since the coupling strength of $A\ ^2\Sigma^+/X\ ^2\Pi$ is much stronger than that of $A\ ^2\Sigma^+/1\ ^4\Pi$, the channel-switching effect observed by Xu *et al.*[40] was attributed to the overwhelming competition of the $N(^2D)$ channel over the $N(^4S)$ channel, as soon as the opening of the $N(^2D)$ channel is energetically possible. However, in both Richard-Viard's[31] and Xu's[40] experimental studies, the total released kinetic energies of NO^+ fragments were measured by simulating the time-of-flight (TOF) profiles to determine the state distributions. Since this is a low resolution method for obtaining the fragment state distribution, detailed information about the dissociation dynamics may be buried.

In present work, we extended Xu's photodissociation study[40] of $N_2O^+(A\ ^2\Sigma^+)$ by using ion velocity imaging, which is a precise method to measure the total released kinetic energy distribution of NO^+ fragments. By analyzing the velocity distributions, we found three kinds of NO^+ fragments with different internal state distributions. With the help of potential energy surfaces (PESs), three dissociation pathways of $N_2O^+(A\ ^2\Sigma^+)$ were proposed to interpret our observations.

II. EXPERIMENT

The experimental setup had been described in detail previously.[42,43] Briefly, sample of ~20% N_2O/He gas mixture at a stagnation pressure of 2 atm was expanded supersonically into a vacuum chamber through a pulsed valve (General Valve). The molecular beam was collimated by a skimmer, and then intercepted by two linearly polarized laser beams, the ionization laser and the dissociation laser. The ionization laser was the output of a dye laser (Lambda Physiks LPD3000) with pulse energy of ~5 mJ, and the dissociation laser was the doubled output of another dye laser (Lambda Physiks FL2002) with pulse energy of ~1 mJ. The two lasers, pumped simultaneously by a XeCl excimer laser (Lambda Physiks LPX200, 10 ns) and counterpropagated with each other, were focused by two quartz lens into the vacuum chamber.

The jet-cooled N_2O molecules were ionized through a (3+1) resonance-enhanced multiphoton ionization (REMPI) process at $\lambda=360.55$ nm to generate pure N_2O^+ ions at the vibration-less electronic ground state $X\ ^2\Pi_{3/2,1/2}(000)$.[44] The generated parent ions were excited by the dissociation laser to the predissociative $A\ ^2\Sigma^+$ state in a wavelength range of 280–320 nm. The produced NO^+ fragments were accelerated by the velocity focusing electric fields,[45] and projected onto a dual microchannel plate (MCP) backed by a phosphor screen. The transient images on the phosphor screen were recorded by a thermoelectrically cooled charge coupled device (CCD) camera and accumulated on the CCD chip. The recorded transient images were processed with the event counting procedure by a personal computer to improve the spatial resolution.[46] Simultaneously, the total emission light from the phosphor screen was monitored by a photomultiplier tube (PMT) to optimize the experiment. To eliminate the Doppler effect of N_2O^+ on the velocity image of NO^+ fragments, the wavelength of dissociation laser was scanned across the corresponding vibronic transition band. Since the spatial distribution of the NO^+ fragments was cylindrically symmetric around the electric vector of the dissociation laser, an iterative procedure of inverse Abel transformation was used to reconstruct the initial three-dimensional (3D) velocity distribution of NO^+ fragments.[47]

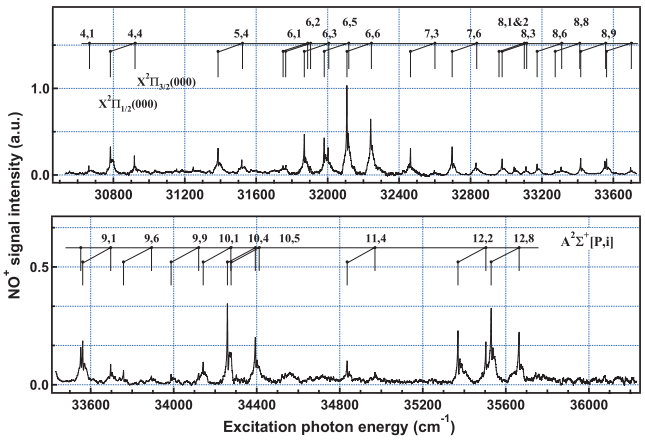

FIG. 2. The PHOFEX spectrum of N_2O^+ ($A\ ^2\Sigma^+ \leftarrow X\ ^2\Pi$) vibronic transition by monitoring the NO^+ fragments. The spectrum is assigned in terms of Fermi-resonance coupled vibrational levels in the $A\ ^2\Sigma^+$ state, $[P,i]$ as defined in Ref. 39. The spectrum helps us to study the dissociation dynamics at specific vibrational levels of $N_2O^+(A\ ^2\Sigma^+)$ with ion velocity imaging technique.

III. RESULTS AND DISCUSSION

A. PHOFEX spectrum of N_2O^+ ($A\ ^2\Sigma^+ \leftarrow X\ ^2\Pi$) transition

In order to fix the wavelength of the dissociation laser for a specific $A\ ^2\Sigma^+ \leftarrow X\ ^2\Pi$ vibronic transition of N_2O^+ ions, the PHOFEX spectrum was obtained by monitoring NO^+ fragments and scanning the wavelength of dissociation laser. The intensities of ionization laser and dissociation laser were carefully optimized in order to make sure that the NO^+ fragments were generated by the cooperative action of the two lasers, not by a single laser. The PHOFEX spectrum, as shown in Fig. 2, is essentially the same as that obtained by Xu *et al.*[39] This spectrum assures that NO^+ fragments are the dissociation products of N_2O^+ ions at the $A\ ^2\Sigma^+$ state.

The vibrational levels of $N_2O^+(A\ ^2\Sigma^+)$ in the PHOFEX spectrum are assigned in terms of $[P,i]$,[39] i.e., the cluster of vibrational levels coupled by Fermi-resonance in the $A\ ^2\Sigma^+$ state among zero-order vibrational levels, (v_1,v_2,v_3), (v_1-1,v_2+2,v_3), and (v_1-2,v_2,v_3+1). Here, P represents the cluster dimension, $P=2v_1+v_2+4v_3$, and i the energy ordering number within the cluster increasing with the energy. With this spectrum, we could study the dissociation dynamics of N_2O^+ at specific vibrational levels of $A\ ^2\Sigma^+$ state with ion velocity imaging technique.

B. Ion velocity imagings and assignments of NO^+ velocity distributions

The ion velocity imagings of NO^+ fragments were obtained at all the vibronic transition peaks of N_2O^+ ($A\ ^2\Sigma^+ \leftarrow X\ ^2\Pi$). Here, we just show some typical examples as in Fig. 3. These imagings are the results of inverse Abel transformation from raw imagings using an iterative procedure for 50 times. The numbers in brackets represent the denotations of vibrational levels [P, i] of the $A\ ^2\Sigma^+$ state as in Fig. 2. As seen from the imagings, all the angular distributions of NO^+ fragments are isotropic, indicating that the $N_2O^+(A\ ^2\Sigma^+)$ ions are predissociative.[48] By accumulating the intensity of NO^+ ions at different velocities in the imagings, the velocity distributions of NO^+ fragments were derived directly, as shown at the right side of Fig. 3.

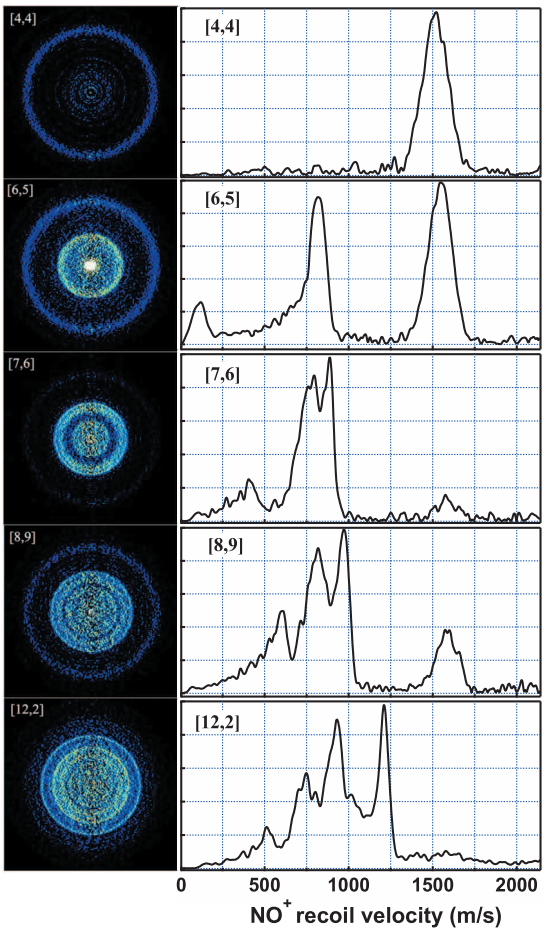

FIG. 3. Inverse Abel transformed ion velocity imagings of NO^+ fragments and the corresponding velocity distributions obtained at different vibrational levels $[P,i]$ of $N_2O^+(A\ ^2\Sigma^+)$. The electric vector of the dissociation laser is parallel to the vertical direction of the image plane.

It is known that there are two dissociation limits to produce NO^+ fragment in present studied energy region, i.e., $NO^+ + N(^4S)$ at 10 430 cm^{-1} [$N(^4S)$ channel] and $NO^+ + N(^2D)$ at 29 660 cm^{-1} [$N(^2D)$ channel].[16] Therefore, it seems apparently that the outer ring of the imagings should correspond to the $N(^4S)$ channel with higher kinetic energy, and the inner ring should be the $N(^2D)$ channel with lower kinetic energy. From these imagings, the variation of dissociation channels with excitation energy or with the vibrational levels of $N_2O^+(A\ ^2\Sigma^+)$ can be clearly seen.

The assignments of NO^+ fragment velocity distributions in terms of internal states are based on the conservations of energy and momentum. From energy conservation, the internal energy of NO^+ fragments, E_{int}, can be obtained with the relation,

$$h\nu - D_0 = E_{int} + E_{tot}, \tag{4}$$

where $h\nu$ is the photon energy of dissociation laser, D_0 is the dissociation limit for a specific channel, and E_{tot} is the total released kinetic energy for NO^+ and N fragments. E_{tot} can be obtained from momentum conservation,

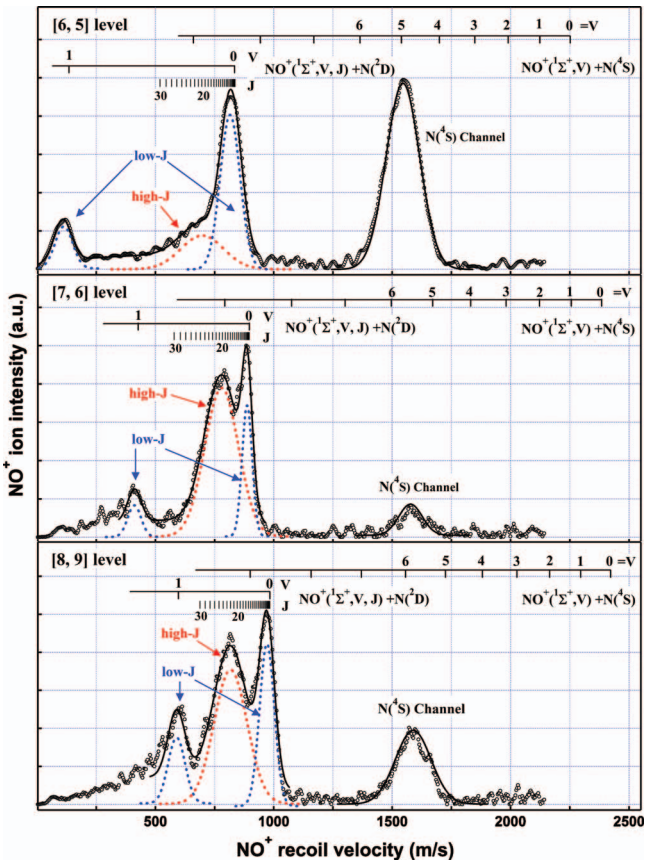

FIG. 4. The assignments of NO^+ velocity distributions obtained at vibrational levels [6,5], [7,6], and [8,9] of $N_2O^+(A\ ^2\Sigma^+)$. In each graph, the circle represents the experimental data, and the solid line represents the fitted result in terms of Gaussian functions (dashed lines). Three velocity distribution components are identified, corresponding respectively to the $N(^4S)$ channel, the $N(^2D)$ channel with low rotational excitation, and high rotational excitation of the NO^+ fragment.

$$m_{NO+}V_{NO+} = m_N V_N, \tag{5}$$

and

$$E_{tot} = 1/2m_{NO+}V_{NO+}{}^2 + 1/2m_N V_N{}^2, \tag{6}$$

where m_{NO+}, m_N, V_{NO+}, and V_N represent, respectively, the masses and velocities of the NO^+ and N fragments. Taking the dissociation limits $D_0 = 10\,430\ cm^{-1}$ for the $N(^4S)$ channel and $D_0 = 29\,660\ cm^{-1}$ for the $N(^2D)$ channel, as well as the vibrational frequency $\nu = 2376.4\ cm^{-1}$ and the rotational constant $B = 1.9973\ cm^{-1}$ of $NO^+(X\ ^1\Sigma^+)$,[16] possible assignments of NO^+ fragment velocity distributions could be given. Due to the great difference between the two dissociation limits, it is straightforward to assign the outer ring of the imagings as the $N(^4S)$ channel and the inner ring as the $N(^2D)$ channel. Therefore, the single velocity distribution peak in Fig. 3, for the dissociation of $N_2O^+(A\ ^2\Sigma^+)$ at the [4,4] vibrational level, is certainly associated with the $N(^4S)$ channel which follows the generally accepted predissociation pathway in Eq. (2). Assignments to the velocity distributions obtained at higher energy levels of $N_2O^+(A\ ^2\Sigma^+)$ were tried in a similar way.

Figure 4 shows the assignments of NO^+ velocity distributions obtained at [6,5], [7,6], and [8,9] vibrational levels of $N_2O^+(A\ ^2\Sigma^+)$. In each graph, the vibrational/rotational state positions of $NO^+(^1\Sigma^+)$ from the $N(^4S)$ and the $N(^2D)$ channels are marked. As can be seen from the figure, for the velocity distribution obtained at [6,5] level, the observed three peaks can be satisfactorily assigned. The peak at 1550 m/s must be the NO^+ fragment from the $N(^4S)$ channel, and its state distribution shows the occurrence of vibrational population inversion centering at v=5, which is consistent with previous works.[23,24,31] The peaks at 810 and 120 m/s are associated with the $N(^2D)$ channel, and can be well assigned to the v=0 and 1 vibrational states of $NO^+(^1\Sigma^+)$. However, the same situation does not hold for the [7,6] and [8,9] vibrational levels. For the velocity distribution obtained at [7,6] level, although the peaks at 1580, 880, and 410 m/s can be satisfactorily assigned to NO^+ (v=5–6) from the $N(^4S)$ channel and NO^+ (v=0 and 1) from the $N(^2D)$ channel, an additional peak at 780 m/s in between the NO^+ (v=0 and 1) peaks cannot be well assigned. This additional peak also exists in the velocity distribution obtained at the [8,9] level, and can be assigned neither. In fact, this peak also exists in the velocity distribution of the [6,5] level, as seen from the deconvoluted results with summation of three Gaussian functions in Fig. 4. Therefore, the key point here is how to assign this peak located in the inner part of the NO^+ imagings.

If inspecting the velocity distributions further, one may notice that the widths of these unknown peaks are much broader than those from the $N(^2D)$ channel, and are almost the same as those from the $N(^4S)$ channel. Broader peak in the velocity distribution indicates that the corresponding fragment NO^+ is rotationally hot, or highly rotationally excited. Therefore, at first glance it is reasonable to assign these unknown peaks as NO^+ fragments from the $N(^4S)$ channel. If so, the corresponding NO^+ will populate at v=8–10, as seen from Fig. 4. In this case, there are two velocity distribution components of NO^+ fragments from the $N(^4S)$ channel. Both of them are rotationally hot, but populate respectively at lower and higher vibrational states. It can be seen from the potential energy curves of N_2O^+ in Fig. 1 that the $NO^+(^1\Sigma^+)+N(^4S)$ dissociation limit correlates adiabatically with the dissociative $1\ ^4\Sigma^-$ state, and the $1\ ^4\Sigma^-$ state crosses with the $X\ ^2\Pi$, the $1\ ^4\Pi$, and the $B\ ^2\Pi$ states. Therefore, predissociation of $N_2O^+(A\ ^2\Sigma^+)$ may be caused by interactions with the $X\ ^2\Pi$, $1\ ^4\Pi$, and $B\ ^2\Pi$ states. Theoretical calculations showed that the crossing between the $A\ ^2\Sigma^+$ and the $B\ ^2\Pi$ states is located very close to the equilibrium geometry of the $B\ ^2\Pi$ state,[15] which is energetically inaccessible in present study and should not be considered as a predissociation origin. Dissociation of $N_2O^+(A\ ^2\Sigma^+)$ via coupling first with the $1\ ^4\Pi$ state and then with the $1\ ^4\Sigma^-$ state is the well known pathway to form NO^+ fragments whose populations center at lower vibrational states (out ring in the imaging). Therefore, the only way to form the NO^+ fragment at higher vibrational state is the predissociation via the $X\ ^2\Pi$ state, i.e., $A\ ^2\Sigma^+ \rightarrow X\ ^2\Pi \rightarrow 1\ ^4\Sigma^- \rightarrow NO^+ + N(^4S)$. If this pathway really exists, since the crossing point between $1\ ^4\Sigma^-$ and $X\ ^2\Pi$ states is lower than that between the $1\ ^4\Sigma^-$ and $1\ ^4\Pi$ states, the generated NO^+ fragment populating at higher vibrational state should be observed earlier than that populating at lower vibrational state, and should also be observed earlier than NO^+ from the $N(^2D)$ channel. This is contrary to our obser-

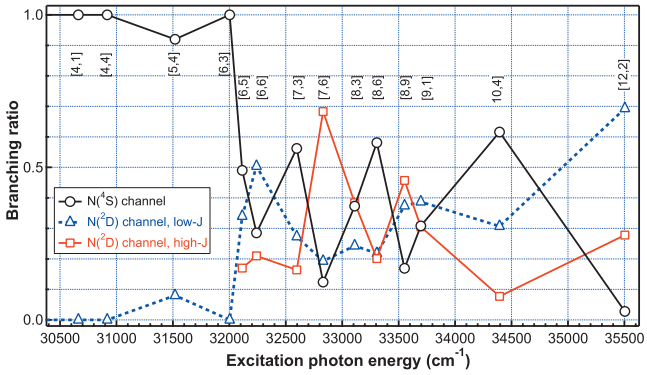

FIG. 5. Variation of the branching ratios for three dissociation pathways to form NO^+ fragment as a function of excitation energy: (○) the $N(^4S)$ channel, (△) rotationally cold NO^+ from the $N(^2D)$ channel, (□) rotationally hot NO^+ from the $N(^2D)$ channel, obtained from the NO^+ velocity distributions at different vibrational levels $[P,i]$ of $N_2O^+(A\ ^1\Sigma^+)$ as in Fig. 4. The branching ratios of the $N(^4S)$ channel and the rotationally hot NO^+ from the $N(^2D)$ channel fluctuate in an opposite way, indicating they endure the same initial dissociation procedure and compete with each other in the final stage.

vations and also the previous experimental results.[23,24,31] Based on these considerations, the unknown peak in Fig. 4 cannot be suitably assigned as NO^+ fragment from the $N(^4S)$ channel, and has to be assigned as the rotationally hot NO^+ fragment from the $N(^2D)$ channel. In summary, there are three types of NO^+ fragments from the dissociation of $N_2O^+(A\ ^2\Sigma^+)$ at higher vibrational levels. One is from the $N(^4S)$ channel with highly rotational excitation, the other two are both from the $N(^2D)$ channel but with different rotational excitations, low-J and high-J, as assigned in Fig. 4. This means that the rotational excitation of the NO^+ product sometimes has bimodal distribution. Consequently, there exist three dissociation pathways of $N_2O^+(A\ ^2\Sigma^+)$ state to form $NO^+ + N$.

C. Branching ratios of three pathways

By fitting the velocity distribution of the NO^+ fragments with Gaussian functions and calculating the area of each deconvoluted peak, the branching ratios of three dissociation pathways were determined and presented in Fig. 5. As can be seen from this figure, at excitation energies below the [5,4] vibrational level of $N_2O^+(A\ ^2\Sigma^+)$, only the first dissociation channel exists, i.e., the $N(^4S)$ channel. The second dissociation channel, the $N(^2D)$ channel, starts to appear at excitation energies above the [5,4] level, especially the [6,3] level at 32 003 cm^{-1} above the vibrationless ground state $X\ ^2\Pi_{3/2}(000)$. Since the appearance energy of the $N(^2D)$ channel is higher than its dissociation limit (29 660 cm^{-1}), there must exist a potential barrier along the $N-NO^+$ bond stretching to form NO^+ and $N(^2D)$. Theoretically calculated potential energy curves in Fig. 1 show a flat barrier near the dissociation exit of the $X\ ^2\Pi$ state. The barrier height was determined from Fig. 5 to be around 2343 cm^{-1}, which had not been experimentally determined previously.

Figure 5 shows that the branching ratios of the three dissociation pathways fluctuate strongly with the vibrational levels of $N_2O^+(A\ ^2\Sigma^+)$, as soon as the $N(^2D)$ channel is opened. This fluctuation may be related to the vibrational modes which are excited at different vibrational levels, or caused by the locations of different vibrational levels which affect the coupling strengths of $N_2O^+(A\ ^2\Sigma^+)$ with other electronic states. An accurate picture for the cause of this fluctuation is hard to obtain at the present stage due to the lack of detailed potential energy surface of the $A\ ^2\Sigma^+$ state and its interactions with neighboring electronic states. It is interesting to notice that the branching ratios of the $N(^4S)$ channel and the rotationally hot NO^+ from the $N(^2D)$ channel fluctuate in an opposite way. This behavior provides a hint that the corresponding two pathways may compete with each other. As will be seen in Sec. III D, these two pathways undergo the same initial dissociation procedure and branch into two parts in the final stage.

D. Predissociation mechanism of $N_2O^+(A\ ^2\Sigma^+)$

As stated in the final part of Sec. III B, rotationally hot NO^+ fragments come from two dissociation channels, the $N(^4S)$ channel and the $N(^2D)$ channel, and rotationally cool NO^+ fragments are from the $N(^2D)$ channel. Dissociation pathway of the $N(^4S)$ channel follows the generally accepted procedure in Eq. (2). Formation of rotationally hot NO^+ from the $N(^2D)$ channel is newly identified in the present study, and its pathway may be inferred from the potential energy curves and is supported from the current experimental observations. From the potential energy curves in Fig. 1, two electronic states correlate adiabatically to the dissociation limit $NO^+(^1\Sigma^+)+N(^2D)$, the $^2\Sigma^-/^2\Delta$ state and the $X\ ^2\Pi$ state. The dissociative $^2\Sigma^-/^2\Delta$ state crosses with the bound $1\ ^4\Pi$ state, and the $1\ ^4\Pi$ state interacts with the $A\ ^2\Sigma^+$ state through a spin-orbit coupling. Therefore, the dissociation pathways of $N_2O^+(A\ ^2\Sigma^+)$ to form the rotationally hot $NO^+(^1\Sigma^+)$ fragment from the $N(^2D)$ channel can be expressed as

$$\begin{aligned} N_2O^+(A\ ^2\Sigma^+) &\overset{\text{spin-orbit}}{\leftrightarrow} N_2O^+(1\ ^4\Pi) \\ &\rightarrow N_2O^+(^2\Sigma^-/^2\Delta) \\ &\rightarrow NO^+(X\ ^1\Sigma^+) + N(^2D). \end{aligned} \tag{7}$$

The initial procedure of the above dissociation pathway is the same as that of the $N(^4S)$ channel in Eq. (2), and differs only in the final stage. From a wave packet point of view, the initial wave packet created on the PES of the $A\ ^2\Sigma^+$ state passes first along the dissociation path at short bond distance to the PES of the $1\ ^4\Pi$ state, and then at long bond distance the wave packet separates into two parts at the curve crossing regions of the $1\ ^4\Pi$ state to the $1\ ^4\Sigma^-$ and the $^2\Sigma^-/^2\Delta$ states. The two parts continue to move separately on the PESs of the $1\ ^4\Sigma^-$ and the $^2\Sigma^-/^2\Delta$ states, and finally lead to the $NO^+ + N(^4S)$ and $NO^+ + N(^2D)$ product channels. As seen from Fig. 1, since the crossing point of the $1\ ^4\Pi$ state with the $^2\Sigma^-/^2\Delta$ state is higher than that with the $1\ ^4\Sigma^-$ state, the appearance energy of the rotationally hot $NO^+(^1\Sigma^+)$ from the $N(^2D)$ channel should be higher than the $N(^4S)$ channel. Our experimental observation agrees well with this speculation. Furthermore, since the wave packet separates at a region near the exit of the dissociation limit, the energy partitioning of total available excess energy for these two

dissociation pathways should be similar, and the NO^+ fragments should have similar degree of rotational excitation. This is what we have observed in the experiment, in which both kinds of NO^+ fragments are rotationally hot. Moreover, experimental results show that the branching ratios of the two dissociation pathways fluctuate with excitation energy in an opposite way. Since these two pathways originate essentially from the same pathway, they compete with each other, the increase of one pathway leads to the decrease of the other pathway. Finally, theoretical calculations indicate that the equilibrium geometry of the bound $1\ ^4\Pi$ state is bent,[11,15] N_2O^+ ion should be in bent structure prior to dissociation due to the spin-orbit coupling of the linear $A\ ^2\Sigma^+$ state to the bent $1\ ^4\Pi$ state. Dissociation on the bent PES results in rotationally excited NO^+ fragment. Observation of rotationally hot NO^+ fragments from the $N(^4S)$ and the $N(^2D)$ channels clearly supports this argument.

The formation of the rotationally cold NO^+ from the $N(^2D)$ channel follows the dissociation pathway in Eq. (3). Since the equilibrium geometries of the $X\ ^2\Pi$ and the $A\ ^2\Sigma^+$ states are linear, the rotationally cold NO^+ fragment must be the result of N_2O^+ dissociation in the linear structure of the $X\ ^2\Pi$ sate. Therefore, the three dissociation pathways observed in the present study can be summarized as follows:

$$N_2O^+(A\ ^2\Sigma^+)\begin{cases}\overset{\text{spin-orbit}}{\leftrightarrow} N_2O^+(1\ ^4\Pi,\text{bent}) \rightarrow \begin{cases} N_2O^+(1\ ^4\Sigma^-) \rightarrow N(^4S)+NO^+, & \text{rotationally hot,} \quad D_0=1.29\ \text{eV} \\ N_2O^+(^2\Sigma^-/^2\Delta) \rightarrow N(^2D)+NO^+, & \text{rotationally hot} \end{cases} \\ \overset{\text{vibronic}}{\rightarrow} N_2O^+(X\ ^2\Pi,\text{linear}) \longrightarrow N(^2D)+NO^+, & \text{rotationally cold,} \quad D_0=3.68\ \text{eV}. \end{cases}$$

IV. CONCLUSION

In the present study, the predissociation dynamics of the N_2O^+ ions at the $A\ ^2\Sigma^+$ state has been investigated with the ion velocity imaging technique. The pure parent ions, prepared at the ground state $X\ ^2\Pi(000)$ by (3+1) REMPI at 360.55 nm, were excited to different vibrational levels of the predissociative $A\ ^2\Sigma^+$ state in a wavelength range of 280–320 nm. By recording ion velocity images of the NO^+ fragments, the NO^+ velocity distributions were obtained. Assignments to the velocity distributions have been performed. Three kinds of the NO^+ fragments from the dissociation of $N_2O^+(A\ ^2\Sigma^+)$ at different vibrational levels are identified. One is from the $NO^+ + N(^4S)$ channel with highly rotational excitation, the other two are both from the $NO^+ + N(^2D)$ channel but with different degrees of rotational excitation, the rotationally hot and the rotationally cold NO^+ fragments. Consequently, there exist three dissociation pathways of N_2O^+ at the $A\ ^2\Sigma^+$ state to form the NO^+ fragment. The pathway for rotationally hot NO^+ from the $N(^4S)$ channel was attributed to the coupling of the $A\ ^2\Sigma^+$ state to the dissociative state $1\ ^4\Sigma^-$ via a bound $1\ ^4\Pi$ state, the pathway for the rotationally hot NO^+ from the $N(^2D)$ channel was due to the coupling of the $A\ ^2\Sigma^+$ state to the dissociative states $^2\Sigma^-/^2\Delta$ via the $1\ ^4\Pi$ state, and the pathway for the rotationally cold NO^+ from the $N(^2D)$ channel was proposed to be the coupling of the $A\ ^2\Sigma^+$ state with the ground state $X\ ^2\Pi$ and the adiabatic dissociation from the $X\ ^2\Pi$ state. The present experimental observations inspire the need for detailed theoretical calculations of the potential energy surface of $N_2O^+(A\ ^2\Sigma^+)$ and its interactions with nearby electronic states.

ACKNOWLEDGMENTS

H.W. and S.L. would like to appreciate Professor Kopin Liu for fruitful discussions and suggestions. This work was supported by the National Natural Science Foundation of China (NNSFC) (Grant Nos. 20873131 and 20928002), the National Key Basic Research Special Foundation (NKBRSF) (Grant No. 2007CB815204), and the Chinese Academy of Sciences. B.J., D.D., and X.Y. thank the National Science Foundation and the Ministry of Science and Technology of China for support.

[1] J. D. Burley, K. M. Ervin, and P. B. Armentrout, J. Chem. Phys. **86**, 1944 (1987).
[2] X. Li, Y. L. Huang, G. D. Flesch, and C. Y. Ng, J. Chem. Phys. **106**, 1373 (1997).
[3] D. J. Levandier, R. A. Dressler, Y. H. Chiu, and E. Murad, J. Chem. Phys. **111**, 3954 (1999).
[4] D. R. Smith, E. R. Huppi, and J. O. Wise, J. Atmos. Sol.-Terr. Phys. **62**, 1189 (2000).
[5] J. W. Duff and D. R. Smith, J. Atmos. Sol.-Terr. Phys. **62**, 1199 (2000).
[6] J. L. Le Garrec, S. Carles, T. Speck, J. B. A. Mitchell, B. R. Rowe, and E. E. Ferguson, Chem. Phys. Lett. **372**, 485 (2003).
[7] A. Pipano and J. J. Kaufman, J. Chem. Phys. **56**, 5258 (1972).
[8] D. G. Hopper, J. Am. Chem. Soc. **100**, 1019 (1978).
[9] D. G. Hopper, J. Chem. Phys. **72**, 3679 (1980).
[10] J. A. Beswick and M. Horani, Chem. Phys. Lett. **78**, 4 (1981).
[11] D. G. Hopper, J. Chem. Phys. **76**, 1068 (1982).
[12] S. Miret-Artes, G. Delgado-Barrio, O. Atabek, and J. A. Beswick, Chem. Phys. Lett. **98**, 554 (1983).
[13] A. R. Gregory, Chem. Phys. **90**, 63 (1984).
[14] H. Gritli, Z. Benlakhdar, G. Chambaud, and P. Rosmus, Chem. Phys. **178**, 223 (1993).
[15] G. Chambaud, H. Gritli, P. Rosmus, H. J. Werner, and P. J. Knowles, Mol. Phys. **98**, 1793 (2000).
[16] J. H. Callomon and F. Creutzbe, Philos. Trans. R. Soc. London, Ser. A **277**, 157 (1974).
[17] J. P. Maier and F. Thommen, Chem. Phys. **51**, 319 (1980).
[18] D. Klapstein and J. P. Maier, Chem. Phys. Lett. **83**, 590 (1981).
[19] J. F. M. Aarts and J. H. Callomon, Chem. Phys. Lett. **91**, 419 (1982).

[20] I. Tokue, M. Kobayashi, and Y. Ito, J. Chem. Phys. **96**, 7458 (1992).
[21] C. E. Fellows and M. Vervloet, Chem. Phys. **264**, 203 (2001).
[22] S. Abed, M. Broyer, M. Carre, M. L. Gaillard, and M. Larzilliere, Phys. Rev. Lett. **49**, 120 (1982).
[23] S. Abed, M. Broyer, M. Carre, M. L. Gaillard, and M. Larzilliere, Chem. Phys. **74**, 97 (1983).
[24] J. Lermé, S. Abed, M. Larzillière, R. A. Holt, and M. Carré, J. Chem. Phys. **84**, 2167 (1986).
[25] M. Larzillière and Ch. Jungen, Mol. Phys. **67**, 807 (1989).
[26] M. C. Elidrissi, M. Larzilliere, and M. Carre, J. Chem. Phys. **100**, 204 (1994).
[27] R. Frey, B. Gotchev, W. B. Peatman, H. Pollak, and E. W. Schlag, Chem. Phys. Lett. **54**, 411 (1978).
[28] P. M. Dehmer, J. L. Dehmer, and W. A. Chupka, J. Chem. Phys. **73**, 126 (1980).
[29] W. W. Chen, J. B. Liu, and C. Y. Ng, J. Phys. Chem. A **107**, 8086 (2003).
[30] I. Nenner, P. M. Guyon, T. Baer, and T. R. Govers, J. Chem. Phys. **72**, 6587 (1980).
[31] M. Richard-Viard, O. Atabek, O. Dutuit, and P. M. Guyon, J. Chem. Phys. **93**, 8881 (1990).
[32] M. Richard-Viard, A. Delboulbe, and M. Vervloet, Chem. Phys. **209**, 159 (1996).
[33] S. Y. Chiang and C. I. Ma, J. Phys. Chem. A **104**, 1991 (2000).
[34] R. G. Orth and R. C. Dunbar, J. Chem. Phys. **66**, 1616 (1977).
[35] J. Berkowitz and J. H. D. Eland, J. Chem. Phys. **67**, 2740 (1977).
[36] J. L. Olivier, R. Locht, and J. Momigny, Chem. Phys. **68**, 201 (1982).
[37] R. Frey, R. Kakoschke, and E. W. Schlag, Chem. Phys. Lett. **93**, 227 (1982).
[38] P. O. Danis, T. Wyttenbach, and J. P. Maier, J. Chem. Phys. **88**, 3451 (1988).
[39] H. F. Xu, Y. Guo, Q. F. Li, S. L. Liu, X. X. Ma, J. Liang, and H. Y. Li, J. Chem. Phys. **119**, 11609 (2003).
[40] H. F. Xu, Y. Guo, Q. F. Li, Y. Shi, S. L. Liu, and X. X. Ma, J. Chem. Phys. **121**, 3069 (2004).
[41] H. Wang, S. L. Liu, J. Liu, F. Y. Wang, B. Jiang, and X. M. Yang, Acta Phys. Sin. **57**, 796 (2008).
[42] H. F. Xu, Y. Guo, S. L. Liu, X. X. Ma, D. X. Dai, and G. H. Sha, J. Chem. Phys. **117**, 5722 (2002).
[43] J. Liu, F. Y. Wang, H. Wang, B. Jiang, and X. M. Yang, J. Chem. Phys. **122**, 104309 (2005).
[44] C. R. Scheper, J. Kuijt, W. J. Buma, and C. A. de Lange, J. Chem. Phys. **109**, 7844 (1998).
[45] A. Eppink and D. H. Parker, Rev. Sci. Instrum. **68**, 3477 (1997).
[46] B. Y. Chang, R. C. Hoetzlein, J. A. Mueller, J. D. Geiser, and P. L. Houston, Rev. Sci. Instrum. **69**, 1665 (1998).
[47] M. J. J. Vrakking, Rev. Sci. Instrum. **72**, 4084 (2001).
[48] C. Zhou and Y. X. Mo, J. Chem. Phys. **129**, 064312 (2008).